Carbohydrate Polymers 118 (2015) 16–23

Contents lists available at ScienceDirect

Carbohydrate Polymers

journal homepage: www.elsevier.com/locate/carbpol

Preparation and adsorption property of xylan/poly(acrylic acid) magnetic nanocomposite hydrogel adsorbent

Xiao-Feng Sun*, Baichen Liu, Zhanxin Jing, Haihong Wang

MOE Key Lab of Applied Physics and Chemistry in Space, Department of Chemistry, College of Science, Northwestern Polytechnic University, Xi'an 710072, China

ARTICLE INFO

Article history:
Received 17 October 2013
Received in revised form 4 November 2014
Accepted 10 November 2014
Available online 15 November 2014

Keywords:
Xylan
Fe_3O_4 nanoparticles
Adsorbent
Methylene blue

ABSTRACT

Adsorbents based on natural polysaccharides have attracted increasing interest because of their low-cost and biodegradability, particularly, polysaccharide-based nanocomposite adsorbents. In this study the xylan/poly(acrylic acid) magnetic nanocomposite hydrogel adsorbent was prepared from wheat straw xylan and Fe_3O_4 nanoparticles, and its adsorption property was studied on methylene blue removal. The prepared hydrogel adsorbent had a semi-interpenetrating network structure and exhibited a macroporous structure with interconnected porous channels. Super-paramagnetic characteristic behavior was observed from magnetic analysis using a vibrating sample magnetometer. The optimum condition for methylene blue adsorption on the adsorbent was found at pH 8 with an adsorbent dosage of 3 g/L and an initial concentration of 400 mg/L, and the removal percentage reached above 90%. The adsorption isotherm of methylene blue on the prepared hydrogel adsorbent was fitted to the Langmuir model, and the pseudo-second-order kinetic model could describe the adsorption process. All obtained results indicated that the prepared hydrogel adsorbent is promising for water treatment applications.

1. Introduction

Wastewater pollution from paper making, cosmetic, electroplating, smelting and dyeing industries is a serious environment problem (Mittal, Gajbe, & Mittal, 2008; Sui et al., 2012; Ai & Jiang, 2012). Removals of hazardous materials from wastewater have been studied by many researchers. According to previous studies (Liu, Wu, Chiu, Suen, & Chu, 2007; Selcuk, 2005; Kornaros & Lyberators, 2006; Shen, Shen, Wen, Wang, & Liu, 2011), various treatment methods have been used to remove hazardous materials, such as ion exchange, chemical precipitation, membrane filtration and adsorption. Adsorption of hazardous materials on adsorbent is considered to the most effective method for wastewater treatment in terms of cost, ease of operation, flexibility and simplicity of design (Crini & Badot, 2008). Recently, there has been increased interest on adsorbents based on natural polymers because of their low-cost and biodegradability. Natural polymers contain abundant functional groups which are very useful for removing hazardous materials. Cellulose, chitosan and cyclodextrin based adsorbents have been reported and used in the areas, such as drug delivery (Luo, Liu, Zhou, & Zhang, 2009), immobilization of enzyme (Luo & Zhang, 2010) and water treatment (Shen et al., 2011; Luo & Zhang, 2009; Huang, Liu, Zhang, Xu, & Hu, 2012).

Xylan is an abundant polymer in nature, and it was found in hardwood and straw, comprising roughly one-fourth to one-third of most plant materials. Xylan consists mainly of β-1→4 linked xylose unites with other substituents arranged in different proportions, and it has excellent hydrophilicity, biodegradability, and biocompatibility (Ebringerová, Hromadkova, & Heinze, 2005; Oliveira et al., 2010); therefore, xylan has become a very promising raw material for preparing novel materials. We have studied the chemical structure and separation of straw xylan (Sun, Fowler, Rajaratnam, & Zhang, 2010; Sun, Jing, Fowler, Wu, & Rajaratnam, 2011), and straw xylan-based hydrogels with excellent swelling and response properties had been prepared (Sun, Jing, & Wang, 2013a; Sun, Wang, Jing, & Mohanathas, 2013b), and the hydrogels can be applied in medical field and wastewater treatment. However, there are few reports that focused on xylan-based nanocomposite hydrogel.

In our previous paper (Sun, Jing, Wang, & Liu, 2014), physical–chemical properties of xylan/poly(acrylic acid) magnetic nanocomposite hydrogel were studied, and the hydrogel had excellent thermal stability, magnetic- and pH-sensitive properties. The thermal stability of the hydrogels enhanced because of an increase in the contents of xylan and Fe_3O_4 nanoparticles; however, the equilibrium swelling ratio decreased with increasing the

* Corresponding author. Tel.: +86 29133 63909336; fax: +86 29 88431672.
E-mail address: xf001sn@nwpu.edu.cn (X.-F. Sun).

http://dx.doi.org/10.1016/j.carbpol.2014.11.013
0144-8617/

contents of Fe_3O_4 nanoparticles and xylan. This paper investigated the adsorption property of the hydrogel on methylene blue (MB) removal, and the effects of solution pH, adsorbent dosage, initial MB concentration and contact time on MB removal were discussed. The adsorption mechanism was also studied using adsorption isotherm and kinetics models.

2. Experimental

2.1. Materials and reagents

Xylan was prepared according to a previous paper (Sun et al., 2013b) with some modifications in which the hemicellulosic material was further treated using 0.05 mol/L HCl solution at 50 °C at a 1:20 (g/mL) solid to liquid ratio to obtain pure xylan, and the xylan material contained 93% xylose and 5% arabinose. Acrylic acid was purchased from the Tianjin Kermel Chemical Reagent Company in China. *N*,*N*′-Methylenebisacrylamide, ammonium persulfate and anhydrous sodium sulfite were purchased from the Tianjing Hongyan Chemical Reagent Factory in China. $FeCl_3{\cdot}6H_2O$, $FeSO_4{\cdot}7H_2O$ and MB were provided by the Tianjing Tianli Chemical Reagent Factory in China. All other reagents used were of analytical grade.

2.2. Preparation of hydrogel adsorbent

The Fe_3O_4 nanoparticles were prepared using chemical co-precipitation method. $FeCl_3{\cdot}6H_2O$ and $FeSO_4{\cdot}7H_2O$ (mol ratio = 2:1) were dissolved in 150 mL of distilled water, and the solution was transferred into a three neck flask filling using N_2. The pH value of the mixed solution was adjusted to 10.0 using $NH_3{\cdot}H_2O$, and this solution was stirred at 70 °C for 1 h. After the reaction, the black substance was removed using a magnet, and the obtained product was washed using distilled water and ethanol alternately for five times. After drying for 24 h in an oven, the black substance was ground to particles of 120 nm diameter, and Fe_3O_4 nanoparticles were finally prepared for further use.

0.4 g of xylan powder was dissolved in the mixed solution of 9 mL distilled water and 1 mL acrylic acid. 0.02 g of *N*,*N*-methylenebisacrylamide and 0.28 g of Fe_3O_4 nanoparticles were added into the above solution, and the mixture was stirred using mechanical agitation under ultrasonic irradiation. Next, 0.01 g of $(NH_4)_2S_2O_8$ and 0.01 g of $NaSO_3$ were added into the mixture solution. After the reaction finished, the black hydrogel materials were removed and cut into uniform size pieces (0.5 × 0.5 × 0.5 cm), and then, these pieces were soaked in distilled water for 48 h. During this period, it was necessary to change the water regularly for washing away unreacted materials. The prepared hydrogel adsorbent were pre-frozen at −20 °C and then freeze-dried at −50 °C for 48 h. Finally, the xylan/poly(acrylic acid) magnetic hydorgel adsorbent was prepared.

2.3. Characterization of the prepared adsorbent

FT-IR spectroscopy was used to analyze the chemical structure of the prepared hydrogel adsorbent. The ground hydrogel samples were mixed with KBr and then pressed into discs that were analyzed using a FT-IR spectrometer (Nicolet 510) in the range from 4000 to 500 cm^{-1}. The magnetic property of the prepared adsorbent was evaluated using a vibrating sample magnetometer (VSM, Lakeshore 7307), and the hysteresis loop was obtained in a magnetic field varying from −1.5 to +1.5 T. The morphology of the adsorbent was observed on a scanning electron microscope (SEM, SUPRA 55), and the hydrogel samples that swollen in distilled water and the solutions of different MB concentrations were first freeze-dried, and the morphology of the samples was observed and photographed.

The mechanical property of the prepared hydrogels with and without Fe_3O_4 nanoparticles was analyzed. Dynamic mechanical analysis (DMA, TA instrument Q800 179 series) was used to determine the compressive modulus of the swollen hydrogel samples. To reach swelling equilibrium, hydrogels were incubated in distilled water for 24 h at room temperature before test. The disk shaped samples were 1 cm × 0.5 cm (diameter × height) in dimension and were tested in compression mode at 25 °C.

2.4. Adsorption experiment

To evaluate the adsorption property of the prepared adsorbent, MB was chosen to remove from aqueous solution using the adsorbent. The effects of solution pH, adsorbent dosage, and initial MB concentration on the adsorption performance of the prepared adsorbent were tested. Varied numbers of the hydrogel adsorbent sample were added in 10 mL solutions of MB, and the pH values of the MB solutions were adjusted using 0.1 mol/L HCl or NaOH solution, and the solutions were sealed at 25 °C for 48 h. The MB concentrations of the remaining solutions were measured using UV–vis spectrometer at its maximum wavelength of 665 nm. The equilibrium adsorption amount of MB, q_e (mg/g), was calculated using the following equation:

$$q_e = \frac{(C_o - C_e)V}{W} \quad (1)$$

Removal percentage (%) was calculated using the equation:

$$\text{Removal percentage } (\%) = \frac{C_o - C_e}{C_o} \times 100\% \quad (2)$$

where C_o (mg/L) and C_e (mg/L) are the MB concentrations at initial and adsorption equilibrium states, respectively; V (L) represents the volume of MB solution; W (g) is the weight of the adsorbent.

The effect of contact time on MB adsorption was performed as follows: 0.5 g of the prepared hydrogel adsorbent was immersed in a 20 mL solution of MB. The pH value of the MB solution was adjusted using 0.1 mol/L HCl and 0.1 mol/L NaOH. After the certain time intervals, the concentration of MB solution was determined using above method. Adsorption amount of MB, q_t (mg/g), at time t (h) was calculated using the following equation:

$$q_t = \frac{(C_o - C_t)V}{W} \quad (3)$$

where C_t (mg/L) is the MB concentration at adsorption time t (h).

3. Results and discussion

3.1. Chemical structure of the prepared adsorbent

Fig. 1 displays the FT-IR spectra of xylan, hydrogel adsorbent and Fe_3O_4 nanoparticles. The broad band at 3400 cm^{-1} was attributed to the O-H stretching vibration, and the absorption peak at 2930 cm^{-1} originated from the C-H stretching vibration. The FT-IR spectrum of xylan presented a band at 1630 cm^{-1} that arose from the water adsorption, and the sharp absorption peak at 1044 cm^{-1} was assigned to the C—O and C—C stretching and the glycosidic linkage V(C—O—C) contributions, which is the characteristic absorption of xylan (Sun et al., 2013b). The band at 562 cm^{-1} appeared in the FT-IR spectrum of Fe_3O_4, which is related to the vibration of the Fe—O (Luo et al., 2009). However, the Fe—O characteristic peak in the FT-IR spectrum of the prepared adsorbent was shifted to lower wavenumber, which may be a result of physical effect. The band at 1726 cm^{-1} appeared in the FT-IR spectrum of the prepared adsorbent, which arises from carbonyl groups of poly(acrylic acid) (Wang

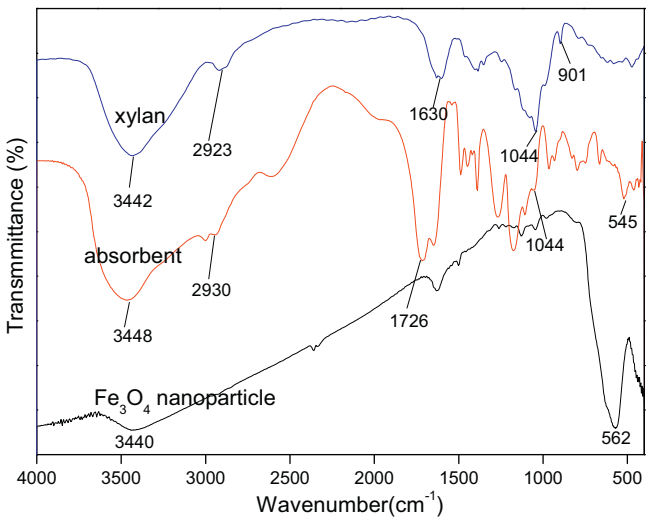

Fig. 1. FT-IR spectra of xylan, hydrogel adsorbent and Fe_3O_4 nanoparticle.

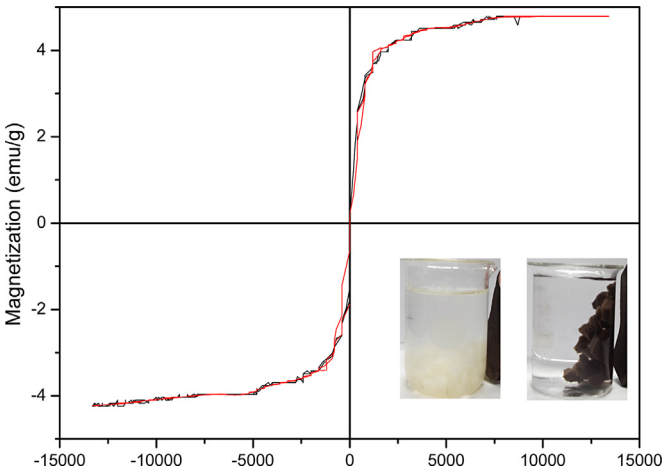

Fig. 2. The magnetic hysteresis loop and photo of the prepared adsorbent.

& Wang, 2010; Li, Ji, Xia, & Li, 2012), and the characteristic absorption peak of xylan was observed at 1044 cm^{-1}, and this indicated that xylans were incorporated into the hydrogel network.

3.2. Magnetic property

Fig. 2 presents the magnetic hysteresis loop and photo of the prepared hydrogel adsorbent. It was observed that the saturation magnetization of the prepared adsorbent was 4.21 emu/g, and the very small magnetization circle was also found, and the coercive force was close to zero, which is the typical characteristic of super-paramagnetic particle (Luo et al., 2009; Luo & Zhang, 2010). The photo of the prepared magnetic hydrogel displays apparent magnetic property under a magnet in comparison with the hydrogel without Fe_3O_4 nanoparticle, and the magnetic hydrogel adsorbent can be separated easily by an external magnetic field. These results indicated that the prepared adsorbent had super-paramagnetic characteristic, which will be very promising in magnetic separation.

3.3. Morphology of the prepared adsorbent

SEM images of the hydrogel adsorbent samples swollen in distilled water and in different MB concentration solutions are displayed in Fig. 3. Fig. 3(e) and (f) shows that Fe_3O_4 nanoparticles were dispersed in the hydrogel adsorbent uniformly. It can be found from Fig. 3(a) that the hydrogel adsorbent exhibited macro-porous structure and interconnect porous channels. The uniform pore distribution was also observed, and this structure is an advantage for improving the adsorption capacity and adsorption rate. Moreover, the pore size of the adsorbent swollen in distilled water was larger than that swollen in MB solutions, and the pore size decreased with increasing MB concentration. The reason may be attributed to the competitive adsorption between MB and H_2O on the surface of the adsorbent. MB is a cationic dye, and it could reduce the repulsion force in the swollen adsorbent because of the electrostatic effect. Therefore, the pore size of the adsorbent decreased with an increase in the MB concentration. Analogous result had been reported in the adsorption of Cu(II) on β-cyclodextrin-based adsorbent (Huang et al., 2012).

3.4. Compressive strength

Fig. 4 displays the stress–strain curves of the hydrogel samples with and without Fe_3O_4 nanoparticles. The prepared magnetic hydrogel presented better compressive strength than that of the hydrogel without Fe_3O_4. Under the stress of 6.984 kPa and a strain of 0.5, the hydrogel sample without Fe_3O_4 failed in compression, and the hydrogel collapsed. Therefore, the addition of Fe_3O_4 nanoparticles enhanced mechanical strength of the prepared hydrogel. The SEM images has presented that the prepared magnetic hydrogel exhibited uniform pore structure and Fe_3O_4 nanoparticles were uniformly dispersed in the hydrogel network; therefore, the mechanical strength was improved significantly.

3.5. Adsorption studies

3.5.1. Effect of pH on adsorption performance of the prepared adsorbent

Fig. 5(a) presents the effect of solution pH on the adsorption performance of the prepared adsorbent. It was observed that both the adsorption amount and the removal percentage of MB first increased and then decreased with increasing pH value from 4 to 10, and both of the adsorption amount and the removal percentage reached the maximum values at pH 8.0 that were 65.28 mg/g and 95.58%, respectively. The carboxyl groups in the hydrogel adsorbent dissociated into $-COO^-$ when increasing solution pH, and the surface of the adsorbent became negatively charged, which would increase the electrostatic attraction between the adsorbent and cationic MB molecule. When the pH value of MB solution was above 8.0, the concentration of Na^+ cation increased, and Na^+ cation would occupy the adsorption site on the adsorbent. Therefore, both of the adsorption amount and the removal percentage of MB decreased at pH above 8.

3.5.2. Effect of adsorbent dosage

The effect of adsorbent dosage on the adsorption performance of the prepared adsorbent is presented in Fig. 5(b). As shown, the removal percentage of MB increased with increasing adsorbent dosage from 0.5 g/L to 6 g/L. When the adsorbent dosage was less than 3 g/L, the increase in the removal percentage was rapid and the removal percentage reached 95% at a dosage of 3 g/L. The increase in the removal percentage was less obvious when increasing adsorbent dosage above 3 g/L, and the adsorption amount of MB gradually decreased from 354.16 mg/g to 32.27 mg/g. The possible reason is that the more adsorbent provided the excessive adsorption sites which may exceed the MB's capacity. Ultimately, a large number of adsorption sites didn't interact with MB molecules.

3.5.3. Effect of initial MB concentration and isotherm studies

Fig. 5(c) presents the effect of initial MB concentration on the adsorption performance of the prepared adsorbent. It was

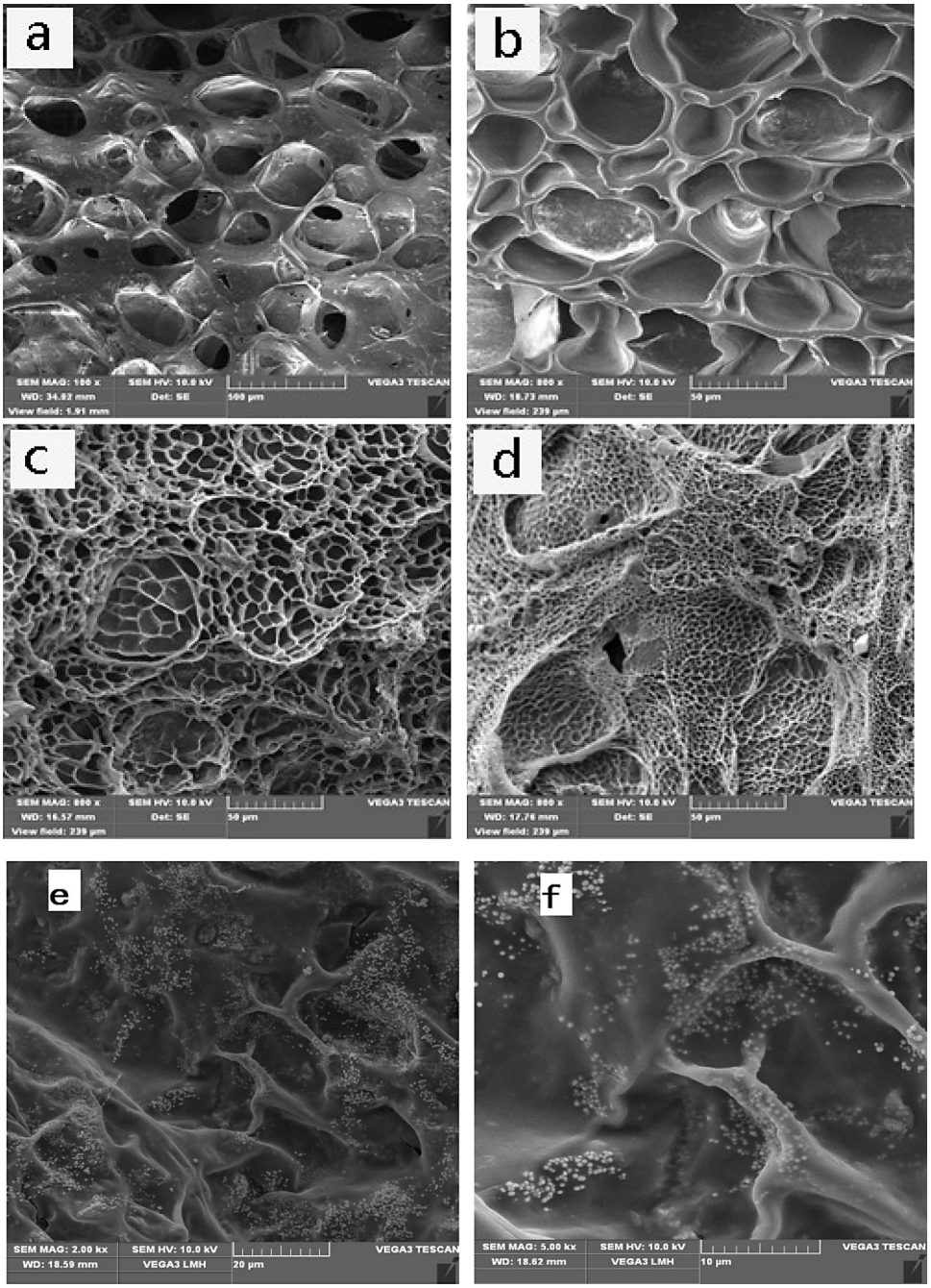

Fig. 3. SEM images of the adsorbent swollen in pH 5.5 distilled water (a, ×100; e, × 2000; f, ×5000), 100 mg/L MB solution at pH 5.7 (b, ×800), 300 mg/L MB solution at pH 6.0 (c, ×800), and 500 mg/L MB solution at pH 6.1 (d, ×800).

observed that the adsorption amount of MB had a linear growth from 15.51 mg/g to 146.92 mg/g as increasing initial MB concentration from 50 mg/L to 500 mg/L. However, the removal percentage decreased with increasing initial MB concentration. The removal percentage of MB slowly decreased when initial MB concentration was less than 400 mg/L, but it kept greater than 93.55%. When further increasing MB concentration, the removal percentage rapidly decreased. A possible reason is that the adsorption sites on the adsorbent were not completely occupied at a low MB concentration, thereby the adsorption amount of MB increased and the change of removal percentage was not obvious. When the concentration of MB solution was higher, the number of MB molecule was beyond the adsorption capacity of the adsorbent, and the decreasing trend of MB removal became rapid.

In order to study the adsorption isotherm of MB on the prepared magnetic nanocomposite adsorbent, the two adsorption isotherms models namely Langmuir and Freundlich were applied to study the equilibrium adsorption data of MB on the prepared adsorbent, and the Langmuir and Freundlich isotherms models are expressed as following Eqs. (4) and (5), respectively (Chen et al., 2013):

$$\frac{C_e}{q_e} = \frac{C_e}{q_{\max}} + \frac{1}{K_L q_{\max}} \tag{4}$$

$$\ln q_e = \ln K_F + \frac{1}{n \ln C_e} \tag{5}$$

where Langmuir isotherm describes a monolayer adsorption on a homogeneous surface; Freundlich isotherm describes the

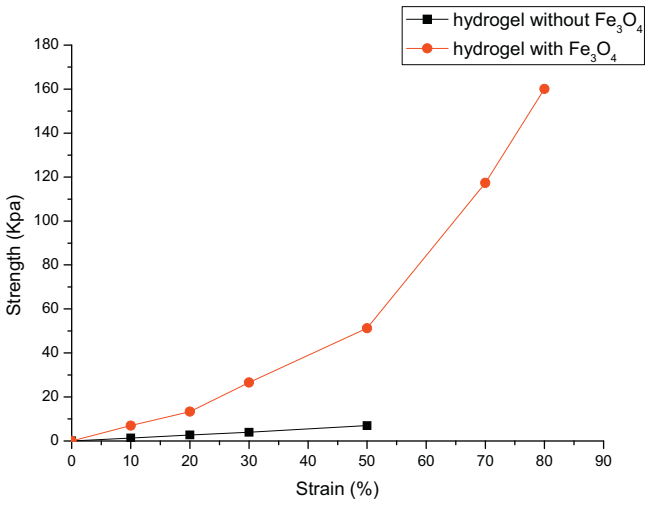

Fig. 4. The stress–strain curves of the hydrogel samples with and without Fe_3O_4.

adsorption on a heterogeneous surface, assuming that the stronger adsorption sites are occupied at first and the adsorption strength decreases with increasing the degree of adsorption site occupation; K_L is the Langmuir adsorption equilibrium constant, which reflects the energy of adsorption; K_F and n are Freundlich characteristic constants that are the indicators of the adsorption and the adsorption intensity, respectively.

The fitted adsorption isotherms graphs are presented in Fig. 6, and the obtained constants using above equations are listed in Table 1. As shown, the correlation coefficient of Langmuir equation was 0.9848, and this indicated that MB molecules were adsorbed on the prepared adsorbent by a monolayer adsorption. The maximum adsorption amount of MB was estimated to be 438.60 mg/g. It

Table 1
Isotherm parameters for MB adsorption on the prepared adsorbent.

Langmuir parameters			Freundlich parameters		
q_e	K_L	R^2	$1/n$	K_F	R^2
438.60	0.01498	0.9848	1.4566	10.6354	0.9100

was also observed that $1/n$ value was 1.4566. According to previous studies (Bulut and Adyın, 2006), the value of $1/n$ in the range of 1 to 10 indicated a good adsorption.

3.5.4. *Effect of contact time and kinetics studies*

Fig. 5(d) presents the effect of contact time on MB removal at different initial MB concentrations. It was observed that the adsorption amount of MB increased with increasing contact time. The adsorption process had two stages: the adsorption behavior at the initial stage was rapid and adsorption equilibrium state reached nearly; the adsorption behavior at the second stage was very slow and it took long time to achieve adsorption equilibrium state. The adsorption time at the initial stage increased as initial MB concentration increased. Similar results had been reported in the studies of the adsorption of MB on chemically modified algal biomass (Rubin, Rodriguez, Herrero, & Sastre de Vicente, 2010) and adsorption of basic dyes onto almond shell (*Prunus dulcis*) (Duran, Ozdes, Gundogdu, & Senturk, 2011).

To investigate the adsorption process and potential rate controlling step, the four kinetics models including the pseudo-first-order kinetic model, the pseudo-second-order kinetic model, Elovich equation and intra-particle diffusion model were used to analyze obtained experimental data. These kinetics equations can be

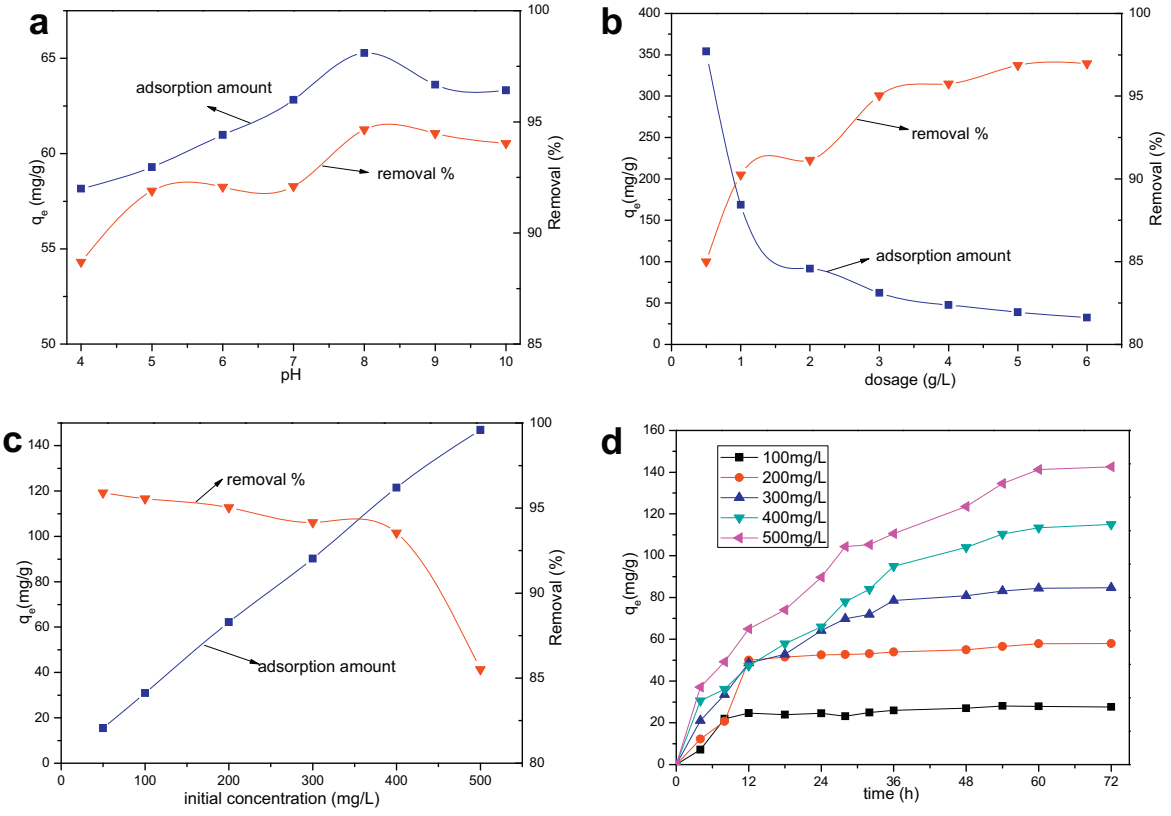

Fig. 5. Effects of adsorption conditions: (a) effect of solution pH; (b) effect of adsorbent dosage; (c) effect of initial concentration; (d) effect of contact time.

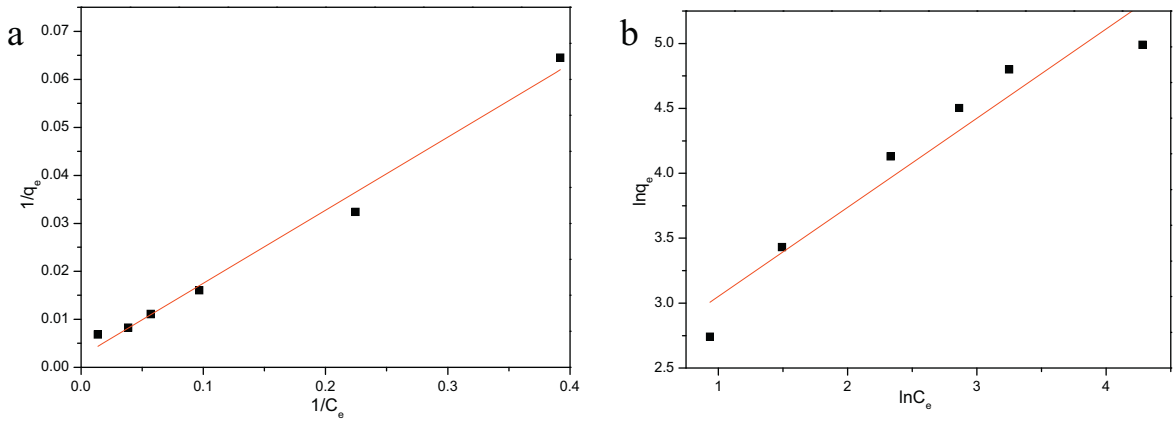

Fig. 6. Adsorption isotherm curves for MB adsorption on the adsorbent.

expressed as follows (Dang, Doan, Dang-Vu, & Lohi, 2009; Yi & Zhang, 2008; Aharoni & Tompkins, 1970):

$$\log(q_e - q_t) = \log q_e - \frac{k_1 t}{2.303} \quad (6)$$

$$\frac{t}{q_t} = \frac{1}{k_2 q_e^2} + \frac{t}{q_t} \quad (7)$$

$$q_t = \frac{1}{b}\ln(ab) + \frac{1}{b}\ln\ t \quad (8)$$

$$q_t = k_i t^{1/2} + c \quad (9)$$

where q_e (mg/g) and q_t (mg/g) are the MB amount adsorbed at equilibrium state and at time t (h), respectively; k_1 (h^{-1}), k_2 (g/mg/h) and k_i (mg/g/$h^{1/2}$) are the rate constants of the pseudo-first-order kinetic model, the pseudo-second-order kinetic model and intra-particle diffusion model, respectively; a (mg/g/h) is the initial adsorption rate, and b (g/mg) is related to the extent of surface coverage and the activation energy for the chemisorption; c (mg/g) is a constant that characterizes boundary layer thickness.

The fitting plots using the four kinetics models are presented in Fig. 7, and the kinetics parameters from fitting results are provided in Table 2. As shown, the correlation coefficient ($R^2 > 0.95$) of the pseudo-second-order kinetic model was greater than that of the pseudo-first-order kinetic model and Elovich equation, which indicates that the pseudo-second-order kinetic model is suitable for describing the adsorption process. This result implied that the overall adsorption process was controlled by chemisorptions. The rate constant k of the pseudo-second-order kinetic model exhibited a reducing trend from 0.00468 to 2.3501×10^{-4} when the initial MB concentration increased from 100 to 500 mg/L, and this result would arise from the decreased competition for adsorption sites at lower MB concentration. Similar result had been reported in the removal of MB from aqueous solution using self-assembled cylindrical grapheme-carbon nantube hybrid (Ai & Jiang, 2012). In addition, the correlation coefficient of Elovich equation presented higher values at higher initial MB concentrations, which is attributed to the higher chemical activation energy, indicating that the adsorption of MB on the adsorbent at higher concentrations also followed the Elovich equation.

Fig. 7(d) presents that the fitted curves didn't pass through the origin, and this indicated that the intra-particle diffusion wasn't the sole rate-limiting step, and the adsorption of MB on the magnetic nanocomposite adsorbent was rather complex and could involve more than one diffusive resistance (Doğan, Alkan, Türkyilmaz, & Özdemir, 2004). It was observed from Table 2 that the correlation coefficient R^2 value increased with increasing initial concentrations, and it arrived to 0.9832 when initial concentration was 500 mg/L. This was related to the porous structure of the adsorbent that offered the channels for the diffusion of MB into the adsorbent, and the driving force also increased at higher MB concentrations.

3.6. Analysis of adsorption mechanism

Fig. 8 presents FT-IR spectra of the adsorbent samples before and after adsorbing MB. Compared to IR spectrum (a), the appearance of the bands at 1556 cm^{-1} and 1452 cm^{-1} in the spectrum (b) of the adsorbent after adsorbing MB was attributed to asymmetric stretching vibration and symmetric stretching vibration of $-COO^-$ groups, respectively (Dragan & Apopei, 2011). This implied that the adsorption of MB on the adsorbent mainly arose from a

Table 2
Adsorption kinetics parameters at different initial MB concentrations.

Kinetics	Parameters	MB concentrations (mg/L)				
		100	200	300	400	500
Pseudo-first-order	q_e[a] (mg/g)	28.10	57.95	84.75	114.94	142.54
	K_1 (h^{-1})	0.06626	0.07862	0.08107	0.06303	0.06126
	q_e[b] (mg/g)	18.7802	48.0198	112.2458	150.4588	183.3370
	R^2	0.9181	0.8280	0.9328	0.9085	0.8376
Pseudo-second-order	q_e[b] (mg/g)	31.0033	68.9976	106.1420	159.9541	186.8204
	K_2	0.00468	0.00131	6.0256E − 4	2.3108E − 4	2.3501E − 4
	R^2	0.9859	0.9570	0.9938	0.9572	0.9786
Elovich equation	a	4.5628	0.3657	0.1276	0.0543	0.0745
	b	0.1776	0.0657	0.0417	0.0296	0.0250
	R^2	0.7424	0.7714	0.9785	0.9368	0.9640
Intraparticle-diffusion	k_i	2.1937	5.9197	10.0233	14.8356	17.4267
	R^2	0.5852	0.6074	0.9093	0.9751	0.9832

[a] Experimental.
[b] Calculated.

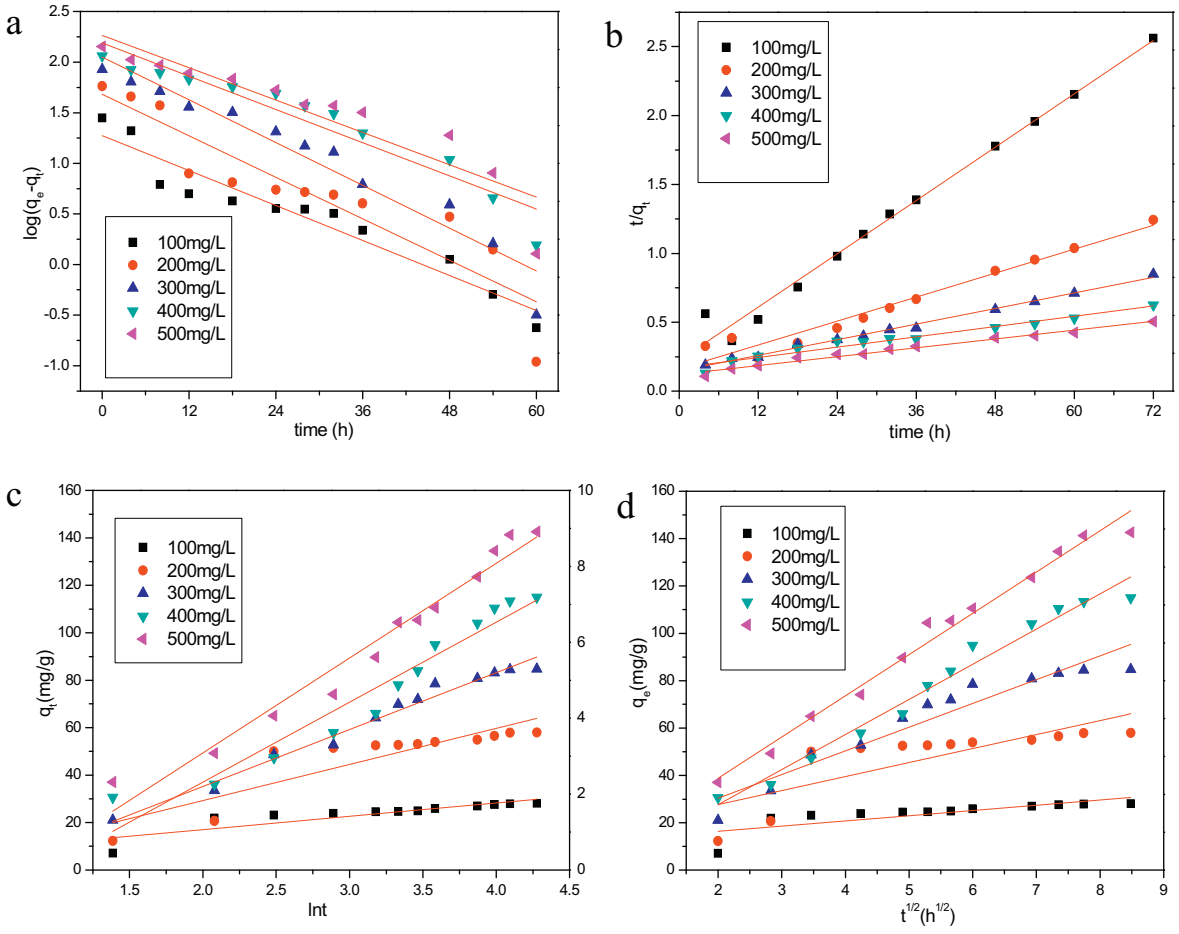

Fig. 7. Kinetics fitted curves: (a) pseudo-first-order kinetic; (b) pseudo-second-order kinetic; (c) Elovich equation; (d) intraparticle-diffusion model.

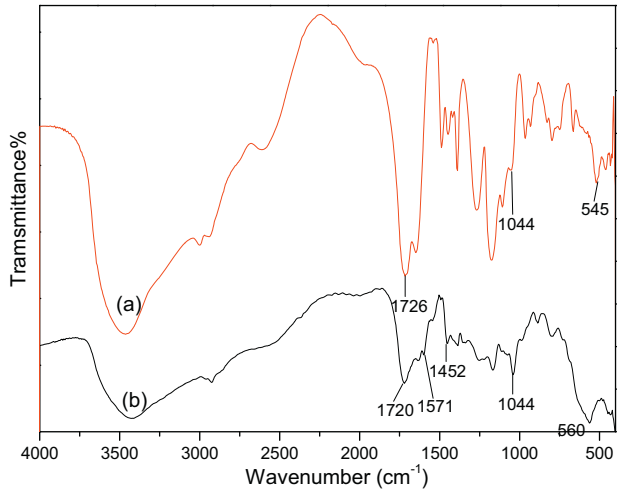

Fig. 8. FT-IR spectra of the adsorbent before and after adsorption: (a) before adsorption; (b) after adsorption.

chemisorption process, and this was in consistent with the result acquired using kinetics models. The poly(acrylic acid) would adsorb MB by electrostatic interaction between carboxylic groups and MB molecules. It was also observed that the Fe—O stretching peak transferred to higher wavenumber after adsorbing MB, which may be related to the physic effect between Fe_3O_4 nanoparticle and MB.

4. Conclusions

The prepared adsorbent exhibited a porous structure and paramagnetic properties, and the introduction of Fe_3O_4 nanoparticle could enable the adsorbent to be separated easily and rapidly from the reaction system by an external magnetic field and also enhance the reusabilty of the xylan-based adsorbent. The adsorption of MB on the adsorbent was affected by solution pH, adsorbent dosage, initial MB concentration and contact time. Adsorption isotherm study indicated that the adsorption of MB on the adsorbent was a monolayer adsorption, and the maximum adsorption capacity was estimated to be 438.60 mg/g. Kinetics study indicated that the pseudo-second order kinetic model could describe the adsorption process, and the adsorption behavior was predicted well using Elovich and intra-particle diffusion equations at higher initial MB concentrations.

Acknowledgements

This work was financially supported by NSFC (no. 20707016), Shaanxi Science and Technology Research Project for Young Scientist (2012KJXX-10), and Fund for Fundamental Research of Northwestern Polytechnical University (NPU-FFR-JC20110274).

References

Ai, L., & Jiang, J. (2012). Removal of methylene blue from aqueous solution with self-assembled cylindrical graphene–carbon nanotube hybrid. *Chemical Engineering Journal, 192*, 156–163.

Aharoni, C., & Tompkins, F. C. (1970). Kinetics of adsorption and desorption and the Elovich equation. In D. D. Eley, H. Pines, & P. B. Weisz (Eds.), *Advance in catalysis and related subjects* (21) (pp. 1–49). New York, NY: Academic Press.

Bulut, Y., & Adyın, H. (2006). A kinetic and thermodynamics study of methylene blue adsorption on wheat shells. *Desalination*, *194*, 259–267.

Chen, Y., Zhai, S., Liu, N., Song, Y., An, Q., & Song, X. W. (2013). Dye removal of activated carbons prepared from NaOH-pretreated rice husks by low-temperature solution-processed carbonization and H_3PO_4 activation. *Bioresource Technology*, *144*, 401–409.

Crini, G., & Badot, P. M. (2008). Application of chitosan, a natural aminopolysaccharide, for dye removal from aqueous solutions by adsorption processes using batch studies: A review of recent literature. *Progress in Polymer Science*, *33*, 399–447.

Dang, V. B. H., Doan, H. D., Dang-Vu, T., & Lohi, A. (2009). Equilibrium and kinetics of biosorption of cadmium(II) and copper ions(II) by wheat straw. *Bioresource Technology*, *100*, 211–219.

Doğan, M., Alkan, M., Türkyilmaz, A., & Özdemir, Y. (2004). Kinetics and mechanism of removal of methylene blue by adsorption onto perlite. *Journal of Hazardous Material*, *B109*, 141–148.

Dragan, E. S., & Apopei, D. F. (2011). Synthesis and swelling behavior of Ph-sensitive semi-interpenetrating polymer network composite hydrogels based on native and modified potatoes starch as potential sorbent for cationic dyes. *Chemical Engineering Journal*, *178*, 252–263.

Duran, C., Ozdes, D., Gundogdu, A., & Senturk, H. B. (2011). Kinetics and isotherm analysis of basic dyes adsorption onto almond shell (*Prunus dulcis*) as a low cost adsorbent. *Journal of Chemical Engineering Data*, *56*, 2136–2147.

Ebringerová, A., Hromadkova, Z., & Heinze, T. (2005). Hemicellulose. *Advances in Polymer Science*, *186*, 1–67.

Huang, Z., Liu, S., Zhang, B., Xu, L., & Hu, X. (2012). Equilibrium and kinetics studies on the adsorption of Cu(II) from the aqueous phase using a β-cyclodextrin-based adsorbent. *Carbohydrate Polymer*, *88*, 609–617.

Kornaros, M., & Lyberators, G. (2006). Biological treatment of wastewater from a dye manufacturing company using a trickling filter. *Journal of Hazardous Material*, *136*, 95–102.

Li, J., Ji, J., Xia, J., & Li, B. (2012). Preparation of konjac glucomannan-based superadsorbent polymers by frontal polymerization. *Carbohydrate Polymers*, *87*, 757–763.

Liu, C. H., Wu, J. S., Chiu, H. C., Suen, S. Y., & Chu, K. H. (2007). Removal of anionic reactive dyes from water from using anion exchange membranes as adsorbers. *Water Research*, *41*, 1491–1500.

Luo, X., Liu, S., Zhou, J., & Zhang, L. (2009). In situ synthesis of Fe_3O_4/cellulose microspheres with magnetic-induced protein delivery. *Journal of Material Chemistry*, *19*, 3538–3545.

Luo, X., & Zhang, L. (2009). High effective adsorption of organic dyes on magnetic cellulose beads entrapping activated carbon. *Journal of Hazardous Material*, *171*, 340–347.

Luo, X., & Zhang, L. (2010). Immobilization of Penicillin G acylase in epoxy-activated magnetic celluose microspheres for improvement of biocatalytic stability and activities. *Biomacromolecules*, *11*, 2896–2903.

Mittal, A., Gajbe, V., & Mittal, J. (2008). Removal and recovery of hazardous triphenymethane dye, methyl violet through adsorption over granulated waste materials. *Journal of Hazardous Material*, *150*, 364–375.

Oliveira, E. E., Silva, A. E., Júnior, T. N., Gomes, M. C. S., Aguiar, L. M., Marcelino, H. R., et al. (2010). Xylan from corn cobs, a promising polymer for drug delivery: Production and characterization. *Bioresource Technolology*, *101*, 5402–5406.

Rubin, E., Rodriguez, P., Herrero, R., & Sastre de Vicente, M. E. (2010). Adsorption of methylene blue on chemically modified algal biomass: Equilibrium, dynamic, and surface data. *Journal of Chemical and Engineering Data*, *55*, 5707–5714.

Selcuk, H. (2005). Decolorization, detoxification of textile wastewater by ozonation and coagulation processes. *Dyes and Pigents*, *64*, 217–222.

Shen, C., Shen, Y., Wen, Y., Wang, H., & Liu, W. (2011). Fast and highly efficient removal of dyes under alkaline conditions using magnetic chitosan–Fe(III) hydrogels. *Water Research*, *45*, 5200–5210.

Sui, K., Li, Y., Liu, R., Zhang, Y., Zhao, X., Liang, H., et al. (2012). Biocomposite fiber of calcium alginate/multi-walled carbon nanotubes with enhanced adsorption properties for ionic dyes. *Carbohydrate Polymers*, *90*, 399–406.

Sun, X. F., Fowler, P., Rajaratnam, M., & Zhang, G. C. (2010). Extraction and characterisation of hemicelluloses from maize stem. *Phytochemical Analysis*, *21*, 406–415.

Sun, X. F., Jing, Z. X., Fowler, P., Wu, Y. G., & Rajaratnam, M. (2011). Structural characterization and isolation of lignin and hemicelluloses from barley straw. *Industrial Crop and Products*, *33*, 588–598.

Sun, X. F., Jing, Z. X., Wang, H. H., & Liu, Y. Y. (2014). Physical–chemical properties of xylan/PAAc magnetic semi-interpenetrating network hydrogel. *Polymer Composites*, http://dx.doi.org/10.1002/pc.23145

Sun, X. F., Jing, Z. X., & Wang, G. Z. (2013). Preparation and swelling behaviors of porous hemicellulose-g-polyacrylamide hydrogels. *Journal of Applied Polymer Science*, *128*, 1861–1870.

Sun, X. F., Wang, H. H., Jing, Z. X., & Mohanathas, R. (2013). Hemicellulose-based pH-sensitive and biodegradable hydrogel for controlled drug delivery. *Carbohydrate Polymer*, *92*, 1357–1366.

Wang, W., & Wang, A. (2010). Synthesis and swelling properties of pH-sensitive semi-IPN superadsorbent hydrogels based on sodium alginate-g-poly(sodium acrylate) and polyvinylpyrrolidone. *Carbohydrate Polymers*, *80*, 1028–1036.

Yi, J. Z., & Zhang, L. M. (2008). Removal of methylene blue dye from aqueous solution by adsorption onto sodium humate/polyacrylamide/clay hybrid hydrogels. *Bioresource Technology*, *99*, 2182–2186.